Analytica Chimica Acta 1317 (2024) 342823

Contents lists available at ScienceDirect

Analytica Chimica Acta

journal homepage: www.elsevier.com/locate/aca

Ratiometric electrochemical aptasensor with strand displacement for insulin detection in blood samples

Lei Zhou [a,b], Ruifeng Zhu [a], Gabriela Figueroa-Miranda [a], Marc Neis [a], Andreas Offenhäusser [a], Dirk Mayer [a,*]

[a] Institute of Biological Information Processing, Bioelectronics (IBI-3), Forschungszentrum Jülich GmbH, Jülich, Germany
[b] Faculty I, RWTH Aachen University, Aachen, Germany

HIGHLIGHTS

- Point-of-care ready electrochemical aptasensor for insulin in diluted blood samples.
- Strongly gold-anchored aptamer' via 2 dithiol-phosphoramidite groups with DNA hybridization to prevent G-quadruplex formation.
- DNA strand displacement during insulin binding induces G-quadruplex formation accompanied by contrary redox signals.

GRAPHICAL ABSTRACT

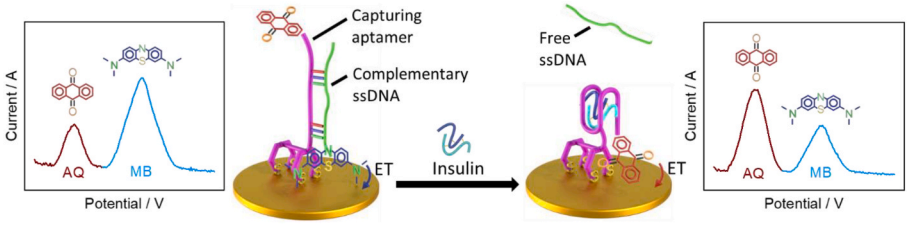

ARTICLE INFO

Handling Editor: Dr Jing-Juan Xu

Keywords:
Atomic force microscopy
Multithiol-immobilization
Ratiometric aptasensor
Insulin detection
Polyethylene glycol
Blood testing

ABSTRACT

Background: Diabetes patients suffer either from insulin deficiency or resistance with a high risk of severe long-term complications, thus the quantitative assessment of insulin level is highly desired for diabetes surveillance and management. Utilizing insulin-capturing aptamers may facilitate the development of affordable biosensors however, their rigid G-quadruplex structures impair conformational changes of the aptamers and diminish the sensor signals.

Results: Here we report on a ratiometric, electrochemical insulin aptasensor which is achieved by hybridization of an insulin-capturing aptamer and a partially complementary ssDNA to break the rigid G-quadruplex structures. To improve the durability of the aptasensor, the capturing aptamer was immobilized on gold electrodes via two dithiol-phosphoramidite functional groups while methoxy-polyethylene glycol thiol was used as a blocking molecule. The exposure of the sensor to insulin-containing solutions induced the dissociation of the hybridized DNA accompanied by a conformational rearrangement of the capturing aptamer back into a G-quadruplex structure. The reliability of sensor readout was improved by the adoption of an AND logic gate utilizing anthraquinone and methylene blue redox probes associated to the aptamer and complementary strand, respectively. Our aptasensor possessed an improved detection limit of 0.15 nM in comparison to aptasensors without strand displacement.

Significance: The sensor was adapted for detection in real blood and is ready for future PoC diagnostics. The capability of monitoring the insulin level in an affordably manner can improve the treatment for an increasing number of patients in developed and developing nations. The utilization of low-cost and versatile aptamer

* Corresponding author. Institute of Biological Information Processing, Bioelectronics (IBI-3), Forschungszentrum Jülich GmbH, Wilhelm-Johnen-Straße 52428, Jülich, Germany.
E-mail address: dirk.mayer@fz-juelich.de (D. Mayer).

https://doi.org/10.1016/j.aca.2024.342823
Received 2 April 2024; Received in revised form 30 May 2024; Accepted 3 June 2024
Available online 11 June 2024

receptors together with the engineering of ratiometric electrochemical signal recording has the potential to considerably advance the current insulin detection technology toward multi-analyte diabetes sensors.

1. Introduction

Insulin is a crucial polypeptide hormone mainly produced, stored, and secreted by exocytosis of β cells from the pancreatic islets, and is crucial for blood sugar level control [1,2]. It was the first fully sequenced protein, which consists of two polypeptide chains with 21 and 30 amino acids. These two chains are coupled via the formation of disulfide bonds between cysteines and exhibit a molecular weight of 5.81 kDa [3]. Enhanced glucose in the blood is the main stimulus of insulin secretion from β cells, which later binds to insulin receptors and triggers cellular glucose uptake [4]. Besides a high glucose level, amino acid and lipid-derived metabolites also mediate directly or indirectly the glucose-stimulated reactions of β cells for insulin secretion [5].

As a primary protein hormone for homeostasis blood glucose control, insulin plays a critical role in the regulation of physiological glycometabolism for fats and carbohydrates, facilitating glucose uptake and maintaining a balanced blood glucose level. Furthermore, it participates in the synthesis of proteins and fats, and the reversal of lipotoxicity and glucotoxicity [6,7]. Human insulin signals cells to absorb glucose from the blood and to store it mainly in the liver when the blood sugar level is higher than humans need while releasing the sugar from the liver to the blood once a glucose shortage occurs. Thus, insulin prevents both hyperglycemia (high blood sugar) and hypoglycemia (low blood sugar) in healthy humans [8,9]. Insulin binds to its receptor, which consists of both α- and β-subunits at the surface of the cell [10]. The insulin signals are transmitted via phosphorylation and protein–protein association activating several structurally related glucose transporter (GLUT) proteins [11]. The dysfunctional insulin secretion activity of β cells is not only related to diabetes but also obesity, cancers, and various types of neurodegenerative diseases [12,13]. Besides serving as a clinical indicator, insulin testing can also be used to confirm the function of transplanted pancreatic islets as well as for doping control among athletes in sports competitions [14,15].

As previously mentioned, the constant hyperglycemia of diabetes patients is caused by insulin deficiency and/or insulin resistance. The former is related to type 1 diabetes and commonly induced by the destruction of β cells, while the latter is attributed to the impairment of insulin activity to regulate glucose uptake. Insulin resistance can occur for both type 2 and poorly managed type 1 diabetes [6,16]. Insulin resistance appears up to 10–15 years before pancreatic cells are not capable of compensating for the declined insulin sensitivity and impaired glucose tolerance, which contribute to the developed type 2 diabetes [17]. Thus, the insulin level for diabetic patients is either lower than that of healthy individuals (ranging from 50 pM to 2 nM) or in an intermittently dysfunctional high level (over 1.5 μM) due to impaired insulin action [18–20]. The early stimulation of insulin secretion could inhibit the rising of sugar levels and lead to a positive function of glucose homeostasis [6]. Therefore, effective determination of insulin levels in the blood is crucial for the early diagnosis of diabetes, disease monitoring, and treatment evaluation [1]. Easy insulin surveillance supported by insulin monitoring could disburden the self-management of insulin therapy and the daily glycemic control of diabetic patients [21]. Additional arguments for a precise adjustment of insulin administration are the high cost of insulin, fears of injections, weight gain as well as prevention of hypoglycemia which can temporarily or permanently impair cognitive functions [22,23]. Therefore, the routine determination of insulin levels in human blood would be of great importance for diabetic patients. To date, various analytical techniques have been developed for clinically quantitative analysis of insulin, typically immunoassays including radioimmunoassay [24], chip-on assay [25], chemiluminescence spectroscopy [26], colorimetric analysis [27], enzyme-linked immunosorbent assay (ELISA) [28], fluorescence spectroscopy [29], and surface plasmon resonance (SPR) [30], as well as chromatographic methods including liquid chromatography-mass spectrometry (LC-MS) [31], high-performance liquid chromatography (HPLC) [32], and capillary electrophoresis [33]. However, most of these methods are not compatible with point-of-care (PoC) testing, for example, LC-MS and HPLC rely on expensive instruments. Others require toxic or expensive reagents, experienced technicians, suffer from either complicated pre-treatment procedures, relatively low selectivity or sensitivity, or time-consuming detection procedures [28,31,32]. Therefore, several electrochemical strategies have been developed for insulin determination due to their inherent merits such as simplified testing procedures, rapid detection, low cost, miniaturization compatibility, high selectivity, and sensitivity [34]. For instance, Y.M. Park et al. have proposed an electrochemical sensor for insulin determination by using a flexible gold nanopillar electrode decorated with insulin-capturing antibodies [35]. M. Khanwalker et al. have established an insulin-sensing platform through the immobilization of an anti-insulin single-chain variable fragment (scFv) as a bioreceptor [36].

Nevertheless, antibodies have been used more commonly as recognition elements but some shortcomings are associated with them as well, such as complex and expensive fabrication, thermal instability, quality variations, and short dynamic detection range [37]. Recently, also aptamers have been employed for insulin detection due to their inherent advantages such as cost-effectiveness, reproducibility in synthesis, high flexibility in designing sequences, and ease of modification. Furthermore, they can possess enriched target binding sites due to their small size and low molecular weight, low immunogenicity, high stability under harsh conditions as well as good reversibility against repeated thermal denaturation and renaturation, which is promising for PoC analysis [38]. Single-stranded DNA (ssDNA) or RNA aptamers are typically in vitro selected and isolated from a synthetic library containing random sequences of nucleic acids through a technique known as systematic evolution of ligands by exponential enrichment (SELEX) [39].

The insulin-capturing ssDNA aptamer employed in this work named IGA3 was obtained via SELEX by Yoshida et al. [40]. The binding of insulin to the aptamer is mediated by several stable G-quadruplex (G4) structures, highly ordered folding motives formed from guanine-rich ssDNA sequences. This IGA3 insulin-capturing aptamer proved to possess a high binding affinity [41] and has been deployed in combination with different transducer systems. M. Liu et al. have designed a graphene/DNA-based colorimetric biosensor for insulin detection and obtained a detection range of 0–600 nM [42]. Z. Hao et al. have developed a graphene field-effect transistor, where the insulin binding induced the formation of G4 structures alternating the electrical conductance of the graphene channel and thus resulting in a K_D value of 35 nM [41]. Y. Wu et al. reported on an electrochemical insulin aptasensor employing methylene blue (MB) redox probe tethered insulin aptamers. A relatively high detection limit of 20 nM was obtained presumably due to only marginal conformational changes during insulin binding [43]. In addition, several aptasensors have been established that use different nanomaterial electrode modifications including mesoporous carbon, MOFs, or AuNPs, improving the detection limits [44–46]. In summary, electrochemical aptasensors with conventional electrodes suffer from high detection limits, while sensors made from nanomaterials are complex to fabricate and possess narrow dynamic detection ranges in this specific case so that they are not capable of covering the variety of concentrations found for insulin among healthy and diabetic individuals.

These electrochemical aptasensors have in common that their signal

mainly results from changes in the conformation of the ssDNA during target binding. The IGA3 insulin aptamer forms G-quadruplex structures which are conserved during insulin binding and limit the detectable signal [43]. To avoid the formation of unfavorable secondary structures that interfere with the desired conformational change, aptamer-ssDNA duplex structures were introduced as the sensing receptor. Here the target is detected through a strand displacement process which facilitates a "signal-on'' detection scheme where the signal increases together with the analyte concentration, Fig. 1A. In this work, we propose an insulin aptasensor utilizing a strand displacement process to prevent the formation of G4 structures in the insulin-free aptamer and to provide a distinct conformational rearrangement during the binding of the analyte. Furthermore, we implemented both a "signal-on'' and a "signal--off'' redox signal processes which prevent false positive signals, enhance the sensor reliability, and suffer less from environmental interferences [47,48]. Therefore, a first redox probe anthraquinone (AQ) was attached to the capturing aptamer on the distal end from the electrode while methylene blue (MB) was linked to the thiol-free complementary ssDNA strand. In the hybridized complex, a straight, G4-free dsDNA was supposed to form with an MB group located close to the electrode surface, while the AQ-tag was exposed to the bulk medium. Hence, the AQ-modified insulin-capturing aptamer and the MB-modified complementary ssDNA served as "signal-on'' and "signal-off'' redox probes, respectively. In the presence of insulin, the complementary DNA hybrid dissociated and the capturing aptamer formed a G4 structure, forcing the AQ probe to engage to the electrode surface while the MB-tagged ssDNA separated from it. Consequently, insulin detection could be realized by measuring the AQ signal decrease and the MB signal enhancement simultaneously. The immobilization of the capturing aptamer on the electrode surface happened through two dithiol-phosphoramidite $(DTPA)_2$ functional groups which contain in total four thiol groups for a strong binding to gold. For the prevention of biofouling in complex samples like serum or blood, methoxy-polyethylene glycol thiols (PEG) were used as blocking material [49].

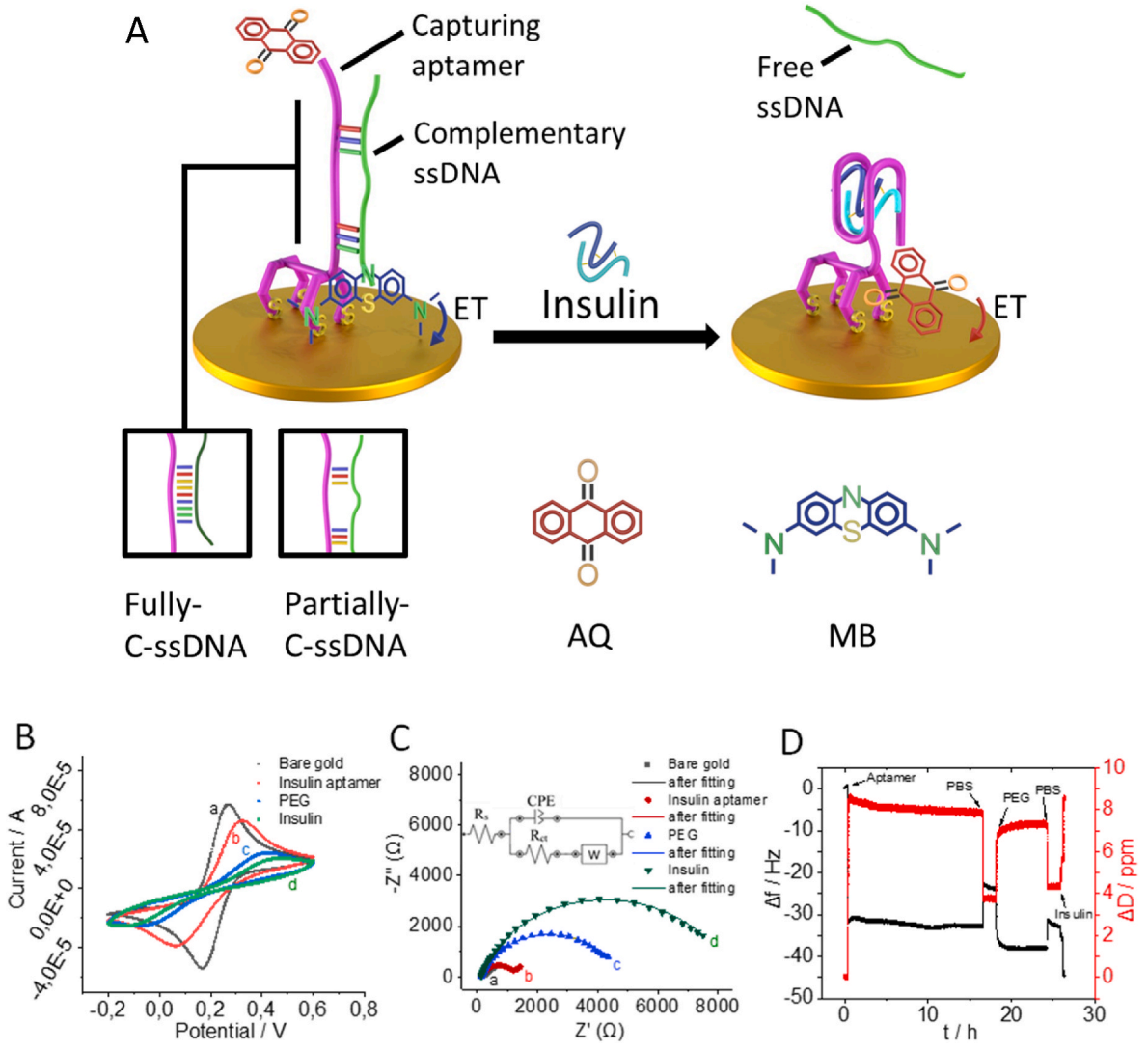

Fig. 1. (A) Illustration of the detection processes through using either full complementary ssDNA or partially complementary ssDNA. (B) CV and (C) EIS results of differently modified electrodes in 10 mM PBS containing 5 mM $[Fe(CN)_6]^{3-/4-}$. The CVs were recorded with a scan rate of 100 mV s^{-1}. The EIS (dots represent experimental data while the lines depict the fitting curves) were conducted with a frequency between 1 Hz and 100 kHz as well as an AC amplitude of 10 mV: (a) bare gold rod electrode, (b) insulin aptamer/PC-ssDNA/gold rod electrode, (c) PEG/insulin aptamer/PC-ssDNA/gold rod electrode, (d) insulin/PEG/insulin aptamer/PC-ssDNA/gold rod electrode. The equivalent circuit model displayed in part (C) contains the solution resistance (R_s), the charge transfer resistance (R_{ct}), a Warburg impedance (*W*), and a constant phase element (*CPE*). (D) QCM-D plot showing the time course of the aptamer immobilization, PEG blocking, and insulin detection. (For interpretation of the references to color in this figure legend, the reader is referred to the Web version of this article.)

2. Material and methods

2.1. Chemicals and apparatuses

The insulin aptamers and (partially) complementary oligonucleotide aptamers employed in this work were synthesized by Friz Biochem GmbH (Neuried, Germany). The human serum albumin aptamers were synthesized on demand by Sangon Biotech Co., Ltd (Shanghai, China). Ethylenediaminetetraacetic acid (EDTA), tris(hydroxymethyl)-aminomethane hydrochloride (Tris-HCl), magnesium chloride, sodium chloride, potassium chloride, sodium phosphate monobasic, sodium phosphate dibasic, 6-mercapto-1-hexanol (MCH), tris(2-carboxyethyl) phosphine hydrochloride (TCEP), potassium ferrocyanide (K_4 [Fe $(CN)_6$]), potassium ferricyanide (K_3 [$Fe(CN)_6$]), hexaammineruthenium (III) chloride ([$Ru(NH_3)_6$]Cl_3), sulfuric acid, hydrochloric acid, sodium hydroxide, human insulin, L-ascorbic acid, thrombin, L-cystine, immunoglobulin G from human serum were all purchased from Sigma-Aldrich Chemie GmbH (Germany) and used without further purification. Gold rod electrodes (2 mm diameter) were ordered from Gaossunion (Wuhan, China), and the Ag/AgCl electrode Dri-Ref-2 was purchased from WPI (Friedberg, Germany). Alumina micro-polish powders (0.05 and 0.3 μm) were provided by Buehler (Leinfelden-Echterdingen, Germany). Isopropanol and ethanol were produced by Merck (Darmstadt, Germany). Monofunctional methoxy-polyethylene glycol thiol (PEG, MW 2 k) was supplied by Creative PEGWorks (Chapel Hill, USA). All these chemical reagents are in analytical grade. The ultra-pure deionized water (18.2 MΩ cm, Milli-Q, Millipore Merck, Darmstadt, Germany) was applied for all experiments involved in solution preparations. The 10 mM Tris-HCl buffer (1 mM EDTA, 10 mM Tris, 100 mM NaCl, pH 8) was prepared for aptamers storage, high salt phosphate buffer solution (10 mM PBS with 10 mM Na_2HPO_4, 10 mM NaH_2PO_4, 1 M NaCl, and 1 mM $MgCl_2$, pH 7.2) was used for aptamer assemblies, low salt phosphate buffer solution (10 mM PBS with 10 mM Na_2HPO_4, 2 mM NaH_2PO_4, 100 mM NaCl, and 3 mM KCl, pH 7.4) was used for electrochemical measurements.

Insulin capturing aptamer sequence (aptamer-ssDNA) [40]:

5′-AQ–$(CH_2)_6$–GGTGGTGGGGGGGGTTGGTAGGGTGTCTTC-$(DTPA)_2$

Complementary ssDNA sequence (*C*-ssDNA):

5′-CATCCCACAG–$(CH_2)_6$–MB.

Partially complementary ssDNA sequence (PC-ssDNA):

5′-CCCCCTTTTTATCCACAG–$(CH_2)_6$–MB.

Specificity test using human serum albumin ssDNA aptamer sequence [50]:

5′-ferrocene–$(CH_2)_6$–GTCTCAGCTACCTTACCGTATGTGGCC-CAAAGCGTCTGGATGGCTATGAA.

-$(CH_2)_6$–*S*–S–$(CH_2)_6$–OH-3’

2.2. Gold rod electrode cleaning

The gold rod electrodes with a diameter of 2 mm were physically and electrochemically cleaned before aptamer immobilization. They were sequentially polished employing alumina powder slurries of 0.3 and 0.05 μm in diameter on micro-cloth pads produced by BASi Research Products (West Lafayette, USA) each for 5 min. Then these well-polished electrodes were consecutively sonicated in ethanol, isopropanol, and Milli-Q water each for 5 min. After sufficient drying in an argon gas stream, electrochemical cleaning was further conducted for these electrodes. Cyclic voltammogram (CV) measurements were firstly carried out in 0.5 M NaOH solution (500 scans with a potential range from −1.35 to −0.35 V and a scan rate of 1 V s^{-1}) and subsequently in 0.5 M H_2SO_4 solution (100 scans with a potential range from −0.15 V to 1.55 V and a scan rate of 1 V s^{-1}) by utilizing PGSTAT302 potentiostat/galvanostat (Metrohm Autolab, Netherlands). The electroactive surface areas of the electrodes were electrochemically determined in 0.5 M freshly prepared H_2SO_4 by cycling the potential between −0.15 V to 1.55 V with a scan rate of 0.1 V s^{-1} until a stable CV was recorded [51]. These electrodes were sufficiently rinsed with Milli-Q water and purged with an argon gas stream before further modifications.

2.3. Aptasensors preparation

The concentration of DNA solutions was determined with a UV/Vis spectrometer (DS-11 Series Spectrophotometer/Fluorometer, DeNovix Inc., Wilmington, DE, USA) by recording the absorbance at 260 nm. The solution of the aptamer was always pre-treated with 10 mM TCEP for 1 h to split the disulfide bonds of the protection group. Subsequently, the solution was diluted to the desired concentrations by high salt PBS to reduce the electrostatic repulsions between ssDNA molecules and facilitate an effective aptamer immobilization.

After those steps described above, the well-cleaned electrodes were immediately soaked in 250 μL aptamer solutions at a defined concentration for 1 h. Either the complementary ssDNA or partially complementary ssDNA (*C*-ssDNA/PC-ssDNA) coexisted with twice the concentration of the insulin-capturing aptamer (aptamer-ssDNA). Afterward, the Au samples were rinsed carefully and extensively with low salt PBS and followed by Milli-Q water to remove non-specifically adsorbed substances including the unhybridized *C*-ssDNA/PC-ssDNA. After purging with argon gas, these electrodes were further immersed in 250 μL 1 mg mL^{-1} PEG dissolved in Milli-Q water for 1 h and carefully washed with low salt PBS and Milli-Q water. PEG functioned as both a blocking agent and spacer material, which can not only eliminate pinholes but also maintain space between receptor molecules for analytes and binding, see below. Aptamer/PEG receptor layers have been proven to effectively preventing biofouling in human serum samples [52]. Noteworthy, PEG causes interference during some characterization experiments such as AFM and chronocoulometry measurements. In these experiments, MCH was used as blocking molecules instead of PEG, which has similar blocking properties in buffer but with low efficiency in complex matrices.

2.4. AFM investigations

All atomic force microscopy (AFM) experiments were conducted with a Nanoscope Multi-mode 8 microscope (Bruker, Germany) utilizing a piezoelectric E-series scanner for sample placement. Aluminum back-coated Si cantilevers from Bruker (RTESPA-3, resonant frequency of 300 kHz) were used for tapping mode imaging at a scan rate of 1 Hz recording 256 × 256 pixels for each image. The scan size ranged from 0.25 to 0.5 μm, which is indicated by the scale bar within the images. A bare gold (111) single-crystal disk was used as a model electrode surface facilitating atomically flat gold terraces for an easy identification of morphological changes during molecule immobilization without interferences from the topography of the electrode. Before usage, the crystal was cleaned by consecutive rinsing it in ethanol, isopropanol, and Milli-Q water. After drying in an Ar stream, the single crystal was flame treated for 10 min in a hydrogen flame and cooled down to room temperature under an argon atmosphere.

2.5. Electrochemical detection of insulin

Cyclic voltammetry (CV) and electrochemical impedance spectroscopy (EIS) were used to investigate the processes of sensor fabrication and the target binding, while square wave voltammetry (SWV) was utilized for the quantitative determination of the analyte. The CV and the EIS measurements were conducted simultaneously utilizing a PGSTAT302 potentiostat/galvanostat equipped with a three-electrode configuration where the aptamer-modified gold rod electrode served as the working electrode, an Ag/AgCl electrode was used as the reference electrode, and a platinum wire was utilized as the counter electrode. CVs were recorded in a potential range from −0.2 V to 0.6 V and a scan rate of 0.1 V s^{-1}. EIS measurements were conducted by exerting a sinusoidal voltage of 0.22 V with an amplitude of 0.01 V and a frequency

range between 1 Hz and 10 kHz. The EIS data was fitted with the NOVA 2.1 software containing a frequency response analyzer (FRA) and the values of fitted modules were obtained from corresponding Randles equivalent circuits. SWV tests were also carried out with the PGSTAT302 potentiostat/galvanostat employing the same three-electrode system. All SWVs were measured with a potential range from −0.85 V to 0.1 V, a potential step of 0.005 V, a modulation amplitude of 0.02 V, and a frequency of 25 Hz.

2.6. Aptamer density determination

To determine the aptamer density on the gold surface, 250 μL of 10 nM insulin-capturing aptamer and 1 mM MCH were sequentially applied to the gold rod electrode each for 1 h each. Afterward, 10 mL Tris buffer (10 mM) was injected into the electrolyte cell. Then argon gas was used to sufficiently purge the buffer in the well-sealed glass cell for 10 min, and the chronocoulometric (CC) test was recorded every 2 min to reach a stable signal. Following these steps, the Tris buffer (10 mM) was spiked with 50 μL $[Ru(NH_3)_6]^{3+}$ (RuHex, 10 mM) to form a combination of 50 μM RuHex/10 mM Tris buffer and purged with argon gas for 10 min. The system was afterward rested for an extra 10 min to equilibrate. Directly after this, the CC measurement was performed every 2 min until a stable signal was achieved. The parameters involved in the CC measurements were 0.2 V and −0.5 V for the initial potential and final potential, respectively, the step number was 2, the pulse width was 0.25 s, and 0.002 s was used as the sample interval.

The total charge (Q_{total}) transferred at the gold surface contains both Faradaic redox charges and non-Faradaic capacitive charges. The capacitive charge of the double layer (Q_{dl}), as well as the total charge (Q_{total}) can be extracted at the intercept for t = 0 corresponding to aptamer-free and aptamer-modified surfaces, respectively, when plotting charge (Q) versus $t^{1/2}$. The amount of RuHex electrostatically adsorbed to the ssDNA aptamer can be calculated as $Q_{ss} = Q_{total}$ - Q_{dl}. This leads to the aptamer density at the gold surface following the equation: $\Gamma_{ss} = (Q_{ss}N_A/nFA)$ (z/m), where N_A is Avogadro's number, n represents the number of electrons for a single reaction, F is the Faraday constant, A indicates the effective area of the gold electrode, z represents the charge of redox molecules, m indicates the number of nucleotides of the aptamer. The number of ssDNA tethered redox groups immobilized to the electrode molecules can be also extracted from CVs, which were measured before and after RuHex addition of the CC experiments, according to the following parameters: potential range from −0.5 V to 0.2 V, scan rate of 0.1 V s^{-1}, sample interval of 0.001 V.

2.7. Quartz crystal microbalance (QCM) measurements

The receptor and blocking molecule immobilization as well as the analyte binding were examined by QCM measurements on a quartz crystal microbalance with dissipation monitoring (QCM-D, QSense from Biolin Scientific, Gothenburg, Sweden), which was equipped with a peristaltic microfluidic system. Ahead of measurements, the gold sensor and related parts of its holder were all cleaned obeying the instructions of the QCM-D. The gold chip was first cleaned by using an oxygen plasma with an O_2 pressure of 0.5 mbar and 50 % power for 3 min. Afterward, the formed gold oxide was reduced by an ethanol treatment for 30 min. Then, the sensor was assembled to the holder (cell) and fixed in the QCM-D module. Directly after that, the buffer solution was pumped through the cell from a 2 mL vial until stable signals were obtained. Finally, the frequency and dissipation responses were simultaneously and continuously recorded in real-time by sequentially pumping the respective molecule solutions and washing buffers through the QCM-D cell.

3. Results and discussion

3.1. Characterization of aptasensor fabrication

The stepwise modification of the gold rod electrode for establishing the receptor layer composed of insulin-capturing aptamer (aptamer-ssDNA) and PEG blocking molecule was monitored by cyclic voltammetry (CV) and electrochemical impedance spectroscopy (EIS) in 10 mM PBS containing 5 mM $[Fe(CN)_6]^{3-/4-}$. In CV measurements, the bare gold rod electrode presented a pair of well-defined $[Fe(CN)_6]^{3-/4-}$ redox peaks (black curve). When the hybridized insulin aptamer/PC-ssDNA conjugate was immobilized on the gold rod electrode, the peak currents dropped significantly and the peak potential difference increased (red curve), implying a charge transfer obstruction caused by the electrostatic repulsion between the negatively charged aptamers and $[Fe(CN)_6]^{3-/4-}$. After the modified electrode was further incubated with monofunctional methoxy-polyethylene glycol thiol (PEG), the aptamers uncovered sites were also blocked, thus leading to distinctly decreased redox currents and increased peak potential separation (blue curve). Finally, the incubation of the obtained sensor electrode with insulin caused a further decrease of the peak currents due to steric blocking (green curve), which revealed the binding of insulin to its aptamer (Fig. 1B).

This modification procedure was also studied by EIS measurements using an offset potential of 0.22 V (Ag/AgCl) according to the standard potential of the redox probe. The semicircle diameters in the Nyquist plot correspond to the charge transfer resistance (R_{ct}), and an increased diameter value indicates an increase of the interfacial R_{ct} due to the step-by-step immobilization of either receptors or targets, Fig. 1C. The experimental impedance data were fitted with a Randles equivalent circuit where R_S represents the solution resistance and W accounts for the Warburg impedance reflecting the influence of the redox probes' diffusion on the interface impedance. In addition, a constant phase element (*CPE*) was used as the interface capacitance to better fit the impedance due to the imperfect electrode surface morphology. A small semicircle diameter was observed for the bare electrode (black curve, R_{ct} = 115 Ω), implying a fast charge transfer process without interference from adsorbed molecules. After the self-assembly of the hybridized insulin aptamer/PC-ssDNA on the gold surface, the R_{ct} value increased to 1120 Ω (red curve) owing to the electrostatic repulsion as described above. Moreover, a distinct increased R_{ct} to 4570 Ω (blue curve) was observed after blocking the gold surface with PEG since the charge transfer process of $[Fe(CN)_6]^{3-/4-}$ to the gold surface was hampered by the formed DNA/PEG mixed monolayer. The R_{ct} value increased even further to 8210 Ω (green curve) when insulin was incubated to the modified electrode, which can be ascribed to the steric hindrance of the charge transfer induced by the binding of the analyte. These EIS results were highly consistent with the CV measurements, corroborating that the aptamer receptors and blocking molecules formed a mixed self-assembled monolayer and that insulin can bind to this aptasensor. The isoelectric point (pI) of human insulin is usually considered in a range of 5.2–5.6 [53,54], which is lower in comparison to the buffer and real sample (blood) pH 7.4, suggesting a negative net charge for insulin.

Correspondingly, a net charge of −3/molecule has been reported for human insulin at a pH of 7.4 [55], confirming the assumption of an enhanced charge transfer suppression simultaneously caused by steric blocking and electrostatic repulsion as indicated by the increased R_{ct} values, see also Table S1 for the actual values.

To support the electrochemical experiments of the stepwise immobilization and analyte binding procedures, QCM-D measurements were performed (Fig. 1D). This method reveals the viscoelastic properties of the immobilized bio-receptors on the gold crystal surface by recording the changes of both resonance frequency (f) and dissipation factor (D), reflecting the alteration of mass (thickness) and energy (rigidity/softness) on the sample, respectively [56]. Assisted by an alternating voltage, the quartz crystal was excited into a resonating state at its

resonance frequency. The frequency lowered and the dissipation elevated simultaneously along with the adsorption of molecules, leading to the enhancement of mass and energy in the system [52]. For thin and rigid layers assembled on a planar crystal interface, the change of the resonant frequency (Δf) is proportional to the total loaded mass (Δm) on the crystal surface, which is described by the Sauerbrey equation [57]:

$$\Delta f = -\frac{2{f_0}^2}{A\sqrt{\rho_q \mu_q}}\Delta m \quad (1)$$

Here, Δf is the change in frequency (Hz), f_0 indicates the resonant frequency (Hz) of the fundamental mode, A represents the active area of the crystal surface, ρ_q means the quartz density (2.648 g cm^{-3}), μ_q stands for the shear modulus of the AT-cut quartz crystal (2.947 $\times$ 10^{11} g cm^{-1} s^{-2}), and Δm is the mass loading/release at the surface.

Besides the electrochemical and gravimetrical characterization of the electrode modification, we investigated also the morphological changes induced by the stepwise modification of the gold surface. Here, an ultra-flat gold single crystal, polished to the Au (111) surface, was utilized instead of a polycrystalline rod electrode to unambiguously trace the topography changes during the functionalization of the electrode. Noteworthy, all images are scaled to the same z range (height)

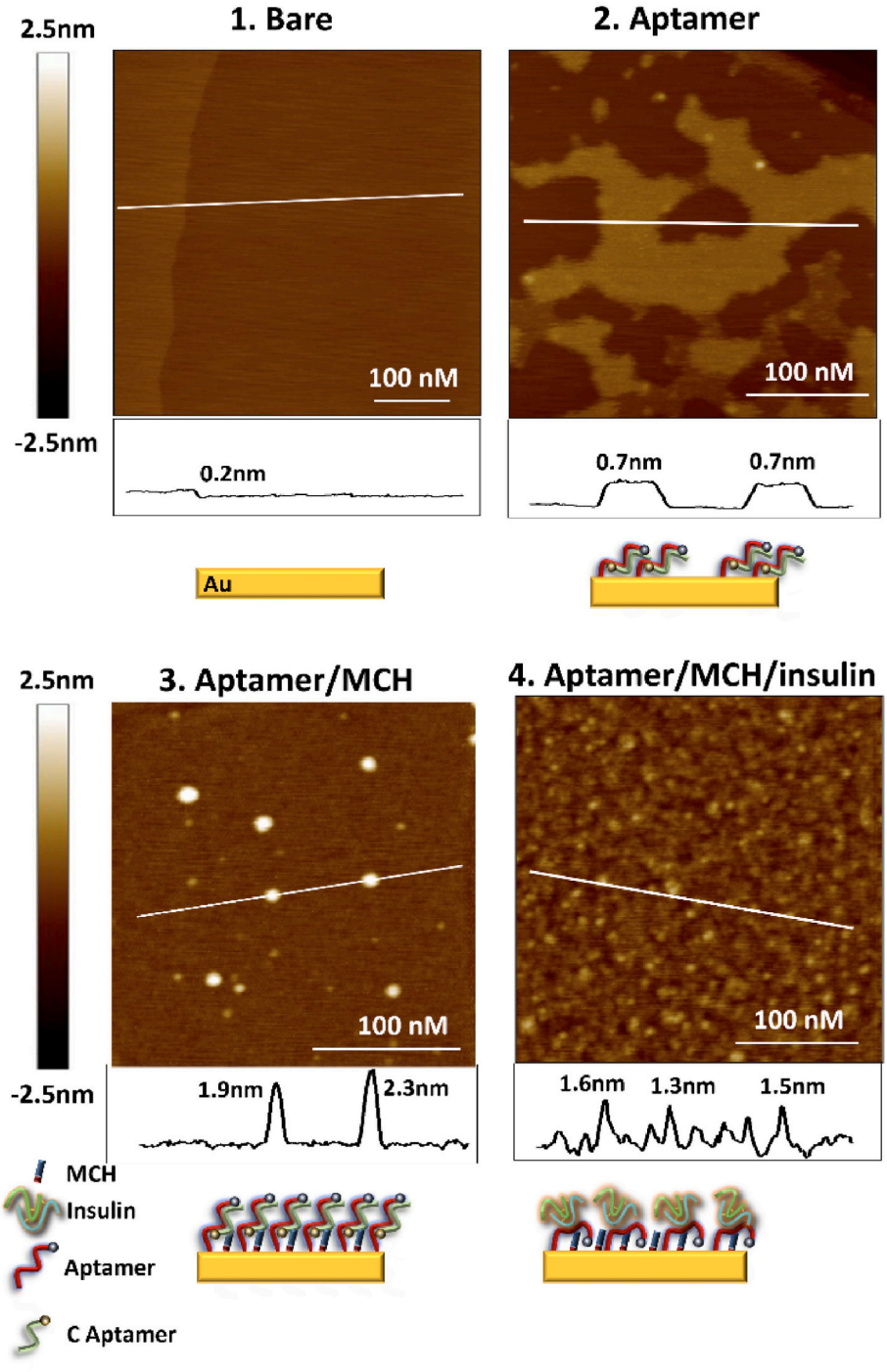

Fig. 2. Tapping mode AFM images of the gold surface before and after aptamer, MCH, and insulin surface immobilization. (For interpretation of the references to color in this figure legend, the reader is referred to the Web version of this article.)

going from - 2.5 to + 2.5 nm, facilitating an easy comparison of the surfaces after the different modification steps and an unambiguous identification of.

Morphological changes occurring during the stepwise modification of the electrode. Before any molecule incubation, the freshly flame-annealed single crystal was investigated by tapping mode AFM. Atomically flat gold terraces with ultra-low roughness of 0.039 ± 0.005 nm were observed (Fig. 2 and Fig. S2). The step edge visible on the left side of the image possessed a height of 0.2 nm corresponding to the gold atom layer distance in (111) direction. In these measurements, even the gold reconstruction can be observed, more pronounced in the phase image than the topography image due to the high z-range, nevertheless proving the high quality of the single crystal preparation and the absence of specifically absorbed molecules as they would lift the reconstruction.

After immobilizing the aptamer-ssDNA/PC-ssDNA conjugate, molecule patches were observed indicating the formation of ordered dsDNA domains, which covered 49 ± 15 % of the gold surface [58,59]. The height of these patches was about 0.7 ± 0.1 nm, which is much smaller than the length of the used DNA. In previous studies, several nanometer-thick monolayers were reported for dsDNA molecules however for higher DNA concentrations and longer incubation times [60]. Under the assembly conditions optimized for our aptasensor, see section 3.2, the dsDNA molecules were presumably lying on the surface. The overall roughness of the samples increased to 0.37 ± 0.02 nm while the areas uncovered by molecules conserved a low roughness of 0.03 ± 0.01 nm suggesting that they remain mainly uncovered by molecules. The elevated structures had a roughness twice as large as the uncovered surface areas.

After MCH incubation, compact molecule films without defects but some elevated structures were found, indicating the full mixing of aptamer and the blocking molecules without phase separations, since both MCH and the DNA molecules share the same mercaptan hexane binding unit. This is also reflected by a decrease in the sample roughness to 0.23 ± 0.02 nm since now the entire surface is covered by the mixed monolayer. It is well-accepted that MCH lifts the DNA molecules from the surface so that the aptamers are tethered to the electrode solely through the thiolate [61]. The roughness of the areas without any elevated objects remained mainly unchanged at 0.075 ± 0.02 nm. The elevated objects represent approximately 3 % of the surface and can be understood as intermolecular DNA aggregates as previously reported for this insulin aptamer [43]. These aggregates vary in size substantially.

After incubation in a 10 μM insulin solution, the morphology noticeably changed and the roughness increased to 0.31 ± 0.01 nm, although the aggregates mainly vanished. The appearance of the surface was more irregular and inhomogeneous with many small elevated and depressed features. After the analyte incubation, the resulting surface appeared similar to electrodes modified with other ssDNA aptamers such as PfLDH (malaria biomarker), glutamate, and AβO (Alzheimer's disease biomarker) aptamers [52,62,63]. The elevated structures were distinctly smaller than those for the previous hybridized aptamer/MCH preparation step, indicating that the aptamer-ssDNA/PC-ssDNA conjugate presumably dissociated due to the interaction of the aptamer with insulin.

Noteworthy, during the stepwise modification with ssDNA aptamers without complementary strands, usually a consecutive increase of the surface roughness can be observed, while in the case reported here, the roughness change between aptamer immobilization and MCH incubation is relatively small [52,62,63]. Just after insulin administration, the roughness slightly increased due to the binding of the analyte to the aptamer-modified electrode and the desorption of the PC-ssDNA. Previously, it was reported that dsDNA monolayers are more compacted and densely packed than ssDNA films, suggesting that the dissociation of the complementary strand initiated by the binding of insulin contributed to the observed roughness increase [60].

3.2. Optimization of analytical performance

To achieve the optimal detection performance for the aptasensor, experimental conditions comprising the immobilization concentration of the insulin aptamer and insulin target incubation time were optimized for a representative analyte concentration of 1 μM insulin. Since the detection performance can be hugely influenced by the packing density of aptamers, the ratiometric oxidation peak currents (I_{AQ}/I_{MB}) extracted from SWV measurements were investigated as a function of the insulin aptamer concentrations. As depicted in Fig. S3A, the value of I_{AQ}/I_{MB} increased with rising concentrations from 1 nM to 10 nM of the insulin aptamer, while this current ratio continuously decreased once the aptamer concentrations exceeded 10 nM. This behavior is reasonable since high concentrations of aptamers on the gold surface can induce steric hindrances as well as electrostatic repulsion effects between neighboring ssDNA molecules and hamper the target analyte recognition or ssDNA stand replacement [55]. Thus 10 nM was selected as the optimal concentration for the incubation of the insulin aptamer and applied for all following experiments. The incubation time of the target biomarker to the biosensor is another important experimental condition that needs to be optimized to facilitate the best performance for the proposed aptasensor. Here, the I_{AQ}/I_{MB} ratio values increased along with the increase of insulin incubation time until they asymptotically approached a plateau after 10 min. No evident change in the I_{AQ}/I_{MB} ratio was witnessed until 25 min, implying a saturation of the insulin binding to the aptasensor (Fig. S3B). Consequently, 10 min was applied as the optimal incubation time for insulin binding and adopted for all following experiments.

3.3. Aptamer density determination

Chronocoulometry (CC) measurements were conducted to estimate the aptamer densities of the insulin aptamers anchored on the gold surface at the previously determined optimal concentration. Therefore, $[Ru(NH_3)_6]^{3+}$ (RuHex) redox probes were employed, which stoichiometrically bind to the anionic phosphates of ssDNA molecules via electrostatic interactions. By applying a potential step crossing the redox potential of RuHex, all charges transferred over the electrode/liquid interface are correlated with the number of self-assembled thiolated aptamer molecules on the gold surface. An insulin aptamer immobilization concentration of 10 nM was evaluated according to the results in Fig. S3A comparison of the extrapolated charge to the time 0 before and after RuHex addition results in a calculated molecule density of 8.49×10^{12} molecules cm^{-2} (Fig. S4), which is in agreement with the QCM data (about 1/3 of all surface molecules were aptamers). The observed molecule density corresponds to a medium aptamer density suggesting that the insulin binding requires moderate interfacial space [64]. These findings were further corroborated by additional CV measurements where the redox peak of capturing aptamer-associated RuHex molecules was used to estimate the molecule density. The CV before RuHex binding showed no clear redox peak since the redox potential of the AQ tag was not reached (Fig. S5A). After RuHex addition a clear redox peak close to −0.2 V occurred which has the typical shape corresponding to surface-immobilized redox groups. The difference in the redox currents before and after RuHex binding were accordingly analyzed yielding a molecule density of 1.09×10^{13} molecules cm^{-2} confirming the CC measurements (Fig. S5). These electrochemical data, suggesting a medium aptamer density, are in agreement with the AFM date observed in section 3.1, where a sub-monolayer of aptamer molecules was observed.

3.4. Ratiometric electrochemical aptasensor

To evaluate the feasibility of the ratiometric aptasensor for insulin detection, SWV measurements were conducted with different modified gold electrodes. SWV signals of electrodes stepwise modified with insulin aptamer/C-ssDNA and PEG (Insulin aptamer/C-ssDNA/PEG/Au

electrode) were recorded from −0.85 V to 0 V in 10 mM PBS (pH 7.4) both before and after insulin incubation. As seen in Fig. S6A, only the *C*-ssDNA associated MB oxidation peak current (black curve) at −0.3 V was detected without insulin, indicating the insulin aptamer was tethered to the gold surface and hybridized with the MB-tagged *C*-ssDNA. After incubation with insulin from 1 nM to 1 μM, an obvious AQ oxidation peak current appeared at about −0.6 V after the exposure to 50 nM insulin and the MB slightly decreased even from lower insulin at 5 nM (light blue and green curve). The signal of AQ reveals that the redox tags were close enough to the electrode surface to get involved in the charge transfer process, while the signal drop of MB was attributed to the binding of insulin to the aptamer and the accompanied dissociation of the hybridization associated with a release of *C*-ssDNA from the insulin aptamer. In the presence of high insulin concentrations of 100 nM, 500 nM, and 1 μM, the oxidation peak currents of MB further decreased and that of AQ correspondingly increased (pink, yellow, and grey curves). Similar tendencies of SWV signals were recorded for insulin aptamer/PC-ssDNA conjugates in combination with PEG modifications (Insulin aptamer/PC-ssDNA/PEG/Au electrode) (Fig. S6B), indicating that both proposed ratiometric.

Electrochemical aptasensors can be used for insulin testing assays. Noteworthy, the ratio of the oxidation peak currents (I_{AQ}/I_{MB}) between AQ and MB was always larger for the partially complementary ssDNA conjugates (aptamer-ssDNA/PC-ssDNA) for every insulin concentration compared with the fully complementary ssDNA (aptamer-ssDNA/C-ssDNA conjugate) presumably due to the lower bonding strength of the partially complementary aptamer-ssDNA duplex [65]. Through the introduction of the complementary ssDNA, the intermolecular G-quadruplex of capturing aptamers is prevented. When the analyte binds to its capturing aptamer hybridized with a complementary ssDNA, the aptamer-protein interactions need to compete not only with the aptamer-ssDNA hybridization but also with intramolecular/intermolecular interactions of the proteins [66]. Such a multi-molecular interaction system can be illustrated by an equilibrium reaction model [67]. Furthermore, fully complementary dsDNA possesses a strong duplex stability competing with the capturing capability of the aptamer, leading to high K_D values. Through introducing mismatching base pairs, the binding strength of the duplex decreases and is less competitive to the aptamer/analyte binding. However, the advantages of using a duplex structure are preserved such as the prevention of G4 structures before insulin exposure, huge conformation change induced by analyte binding, and the low background signal [65]. The sequence of the partially complementary DNA was designed to locate the MB redox tag close to the surface for an easy charge transfer and to bind to the G-rich domain of the capturing aptamer, preventing not only intra but also intermolecular G-quadruplex structure formation. As described in the introduction, this ratiometric aptasensor has high reliability since it uses two redox signals from two redox probes for the analysis of the sensor output, see next section. Thus, the PC-ssDNA was utilized for all following experiments instead of *C*-ssDNA.

3.5. Characterization of the sensor performance

The analytical performance of the proposed dual-redox signal aptasensor for the quantitative insulin determination was evaluated by SWV under optimized conditions (Fig. 3A–D). For blank samples, an obvious MB oxidation peak current can be observed originating from the PC-ssDNA strand. The AQ signal was below the detection limit due to the stretched conformation of the hybridized aptamer and the large distance of AQ from the electrode surface. After incubation of different concentrations of insulin for 10 min, the SWV peak current of AQ (−0.6 V) gradually increased while the SWV response of MB (−0.3 V) continuously decreased along with the increase of insulin concentration. According to the SWV current of AQ and MB, two corresponding linearly related calibration curves can be fitted following the equations below (Table 1), (I_{AQ} and I_{MB} represent AQ and MB peak current, respectively,

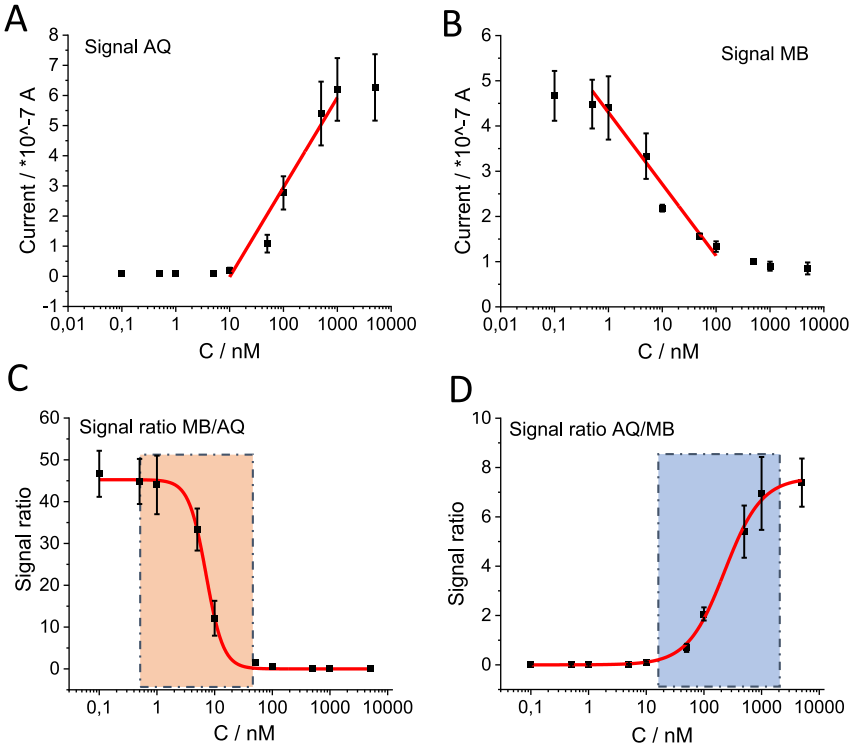

Fig. 3. Calibration curve based on (A) AQ signal, (B) MB signal, (C) MB/AQ signal ratio and (D) AQ/MB signal ratio for insulin aptamer/C-ssDNA/PEG/Au electrode toward insulin with concentrations between 0.1 nM and 10 μM in 10 mM PBS (pH 7.4). For this experiment, three measurements were analyzed and obtained from three different electrodes.

Table 1
Detection characterization.

Detection	Fitting results	Limit of detection (LOD)	Dynamic detection range	Sensitivity
I_{AQ} ($\times 10^{-7}$ A)	3 (lg*C*) – 3 ($R^2 = 0.9838$)	3.3 nM	10 nM-1 μM	0.3 μA nM^{-1}
I_{MB} ($\times 10^{-7}$ A)	−1.6 (lg*C*) + 4.3 ($R^2 = 0.9926$)	0.15 nM	0.5 nM-100 nM	0.16 μA nM^{-1}
Signal ratio $_{(MB/AQ)}$	$45.2 \times (1-(lgC)^{2.89}/(290.3+(lgC)^{2.89}))$ ($R^2 = 0.9986$)	0.8 nM	2.4 nM-45 nM	4.2 nM^{-1}
Signal ratio $_{(AQ/MB)}$	$7.59 \times (lgC)^{1.35}/(1552.6+(lgC)^{1.35})$ ($R^2 = 0.9976$)	4.5 nM	14 nM-2.5 μM	0.005 nM^{-1}

and *C* is the incubated concentration of insulin). Additionally, the insulin adsorption and PC-ssDNA desorption processes can be monitored by the ratio of these redox currents, which follow a Hill equation (Table 1), (*signal ratio* $_{(MB/AQ)}$ means the ratio of peak current between MB and AQ or equivalently the reciprocal *signal ratio* $_{(AQ/MB)}$). The detection limit, dynamic range, and sensitivity extracted from both the peak current-based and signal ratio-based calibration curves are presented in Table 1.

Interestingly, these calibration curves cover different concentration ranges for AQ and MB. This difference can be attributed to the G4 structures formation, indicating that the dissociation of the hybridized aptamer duplex and the insulin analyte binding are two different processes and can be influenced by different factors, respectively [68]. Besides, the confinement of the capturing aptamer to the gold surface may affect its folding into the G4 conformation [69]. Generally, the different concentration ranges are beneficial for the target sensing since the total detection range is highly extended. In our previous work, we found that the detection concentration range can be broadened by jointly utilizing an electrochemical and an optical transducer in the same sensor [70]. In another work, the concentration range was extended by changing the pH of the analyte solution [71]. Here, a similar detection range extension can be achieved however without introducing additional transducer equipment or modifying the analyte, while the reliability is maintained due to the overlap between the two concentration ranges. The overall detection limit and detection range obtained from the combination of MB and AQ redox signals were 0.15 nM and 0.5 nM to 2.5 μM, respectively (Table 1), which covers the hyperinsulinemia diabetic insulin level typically at a full stomach ranging from 2 nM to 1.86 μM as reported previously [20,72,73]. For our sensor, the LOD is 100 times smaller than previously reported by Y. Wu et al. for a sensor without strand displacement [43].

In comparison with other PoC insulin sensors (Table 2), including the comparison with commercially available homogeneous time-resolved fluorescence (HTRF) and ELISA kits, our aptasensor possessed a similar LOD and wider dynamic detection range [74–85]. Moreover, the ratiometric dual-signal mechanism is more reliable for insulin analysis due to the redundant responses. The redox signals of MB and AQ can be treated as an AND logic gate, in which the insulin is used for diagnostic purposes only when both MB and AQ redox currents exhibit a distinct change during testing of the sample (Fig. S7). This logic gate enhances the sensor performance since unspecific interferences of certain chemicals can be eliminated, see next section. As displayed in the truth Table S2, only if both inputs, the signal change of AQ and MB, are not zero, the final electrochemical output signal is trustworthy.

3.6. Selectivity, real sample test, specificity test, stability

To evaluate the selectivity of the developed electrochemical aptasensor to insulin, four potential interfering substances with similar structures to insulin including L-ascorbic acid (L-AA), thrombin (TB), L-cystine (L-CT), and immunoglobulin G (IgG) were investigated in control experiments since they are in parts electroactive and coexist with insulin in human blood. During the tests, we did not observe any apparent AQ redox peak in response to spiking those compounds to the test solutions. Interestingly, these interfering chemicals caused a partial decline of the MB peak currents at certain concentrations, indicating that they are capable of breaking the hybridization and inducing a release of PC-ssDNA strands. However, the missing AQ signal rules out an unspecific binding to the insulin aptamer itself. Nevertheless, the breaking of the hybridization and the decreased peak currents for MB can potentially impair the reliability of the test results. Therefore, we recorded and analyzed these signal drops of MB currents as well as the AQ currents (Fig. S8). In the presence of 10 mM L-ascorbic acid or 10 μM thrombin, which were much higher than physiological concentrations of about 65 μM and 200–780 nM in human blood [86,87], respectively, the signal alterations remained very small for both compounds indicating only a weak interference. However, when the aptasensor was exposed to 100 μM L-cystine or 100 μM IgG, considerable signal drops were observed for the MB redox peak presumably due to unspecific (electrostatic) interactions with the PC-ssDNA. Both L-cystine and IgG possess weak positive charges when they are exposed to the pH of the physiological environment [88]. A reduction of the concentrations to 2 μM for L-cystine and 5 μM for IgG was necessary to eliminate the signal drops. However, the normal concentrations of healthy adults for L-cystine and IgG are around 40 μM and 40–100 μM [89,90], respectively, and thus above those non-interfering levels. This issue could be tackled by a 20-times dilution of the sample, noteworthy, this would increase the LODs of this test. However, the combination of both redox signals (MB and AQ) via an AND logic gate allowed to overcome this problem as these interfering molecules affect only the MB but not the AQ redox response. The final signal ratio of I_{AQ}/I_{MB} showed a huge difference between that of insulin and any of the tested interfering agents (Fig. 4A).

The proposed aptasensor was further evaluated with 20 times diluted real blood samples in comparison with the results from the PBS samples containing the same concentrations of the target analyte.

Table 2
Performance comparison with other PoC strategies for insulin detection.

Detection methods	Limit of detection	Dynamic detection range	References
Optical aptasensor	0.1 nM	0.1 nM-1 nM	[74]
Carbon quantum dots (CQDs)-based electrochemical oxidative detection	2.24 nM	40 nM-200 nM	[75]
NiO Nanoparticles involved in electrochemical oxidative detection	19.6 nM	600 nM-10 μM	[76]
Label-free electrochemical aptasensor	3 nM	10 nM-350 nM	[77]
Synergistically electrocatalytic detection	0.12 nM	0.46 nM-100 nM	[78]
Label-free fluorescent assay	3 nM	10 nM-500 nM, 1 μM-16 μM	[79]
Interferometric reflectance spectroscopy (IRS) optical sensor	32.7 nM	430 nM-8.6 μM	[80]
Aptamer-mediated fluorescent sensor	2.74 nM	4.3 nM-206.4 nM	[81]
Optical porous silicon biosensor	327 nM	860 nM-8.6 μM	[82]
Homogenous time-resolved fluorescence (HTRF)	0.03 nM	0.027 nM-0.21 nM	[83]
ELISA	0.009 nM	0.017 nM-0.17 nM	[83]
ELISA	0.005 nM	0.014 nM-1.4 nM	[84]
ELISA	0.034 nM	0.035 nM-2.25 nM	[85]
Aptasensor	**0.15 nM**	**0.5 nM-2.5 μM**	**This work**

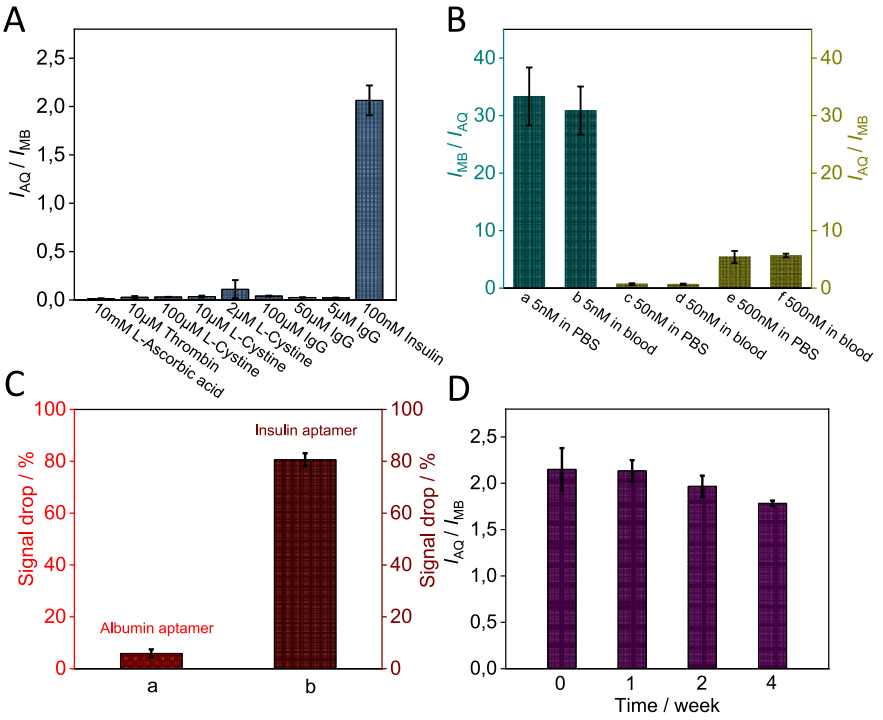

Fig. 4. (A) I_{AQ}/I_{MB} signal ratio of the insulin aptasensor after the exposure to different concentrations of inferences of L-ascorbic acid, thrombin, L-cystine and immunoglobulin G in comparison with the exposure to insulin. (B) I_{MB}/I_{AQ} signal ratio of the insulin aptasensor after the exposure to (a) 10 mM PBS containing 5 nM insulin and (b) 20 times diluted blood samples spiked with 5 nM insulin, (c) 10 mM PBS containing 50 nM insulin and (d) 20 times diluted blood samples spiked with 50 nM insulin, (e) 10 mM PBS containing 500 nM insulin and (f) 20 times diluted blood samples spiked with 500 nM insulin. (C) Signal drop after insulin incubation on (a) albumin aptamer/PEG, and MB peak drop of this (b) insulin aptasensor. (D) I_{AQ}/I_{MB} signal ratio of the insulin aptasensor after stored in the fridge for 1 week, 2 weeks, and 4 weeks. For these experiments, three measurements were analyzed and obtained from three different electrodes.

All blood samples were obtained from a healthy donor via monovette tubes. Ethylenediaminetetraacetic acid (EDTA) was added to avoid blood coagulation. The signal ratios of the two redox tags were obtained from the calibration curves of the SWV signals recorded after incubation in PBS solution and diluted blood spiked with 5 nM, 50 nM, and 500 nM insulin. The I_{MB}/I_{AQ} and I_{AQ}/I_{MB} signal ratios were both determined and utilized either for low, medium, or high concentrations according to their most sensitive parts at the calibration curves, respectively (Fig. 4B). The recoveries at the three concentrations for the real sample measurements were calculated and displayed in Table S3. The high agreement between spiked and measured insulin concentrations rules out interferences originating from blood substances such as human serum albumin, glucose, uric acid, and dopamine as well as other potentially interfering blood-borne components.

Although the real sample test of the insulin aptasensor demonstrated that the unspecific adsorption in complex samples can be eliminated, the specificity of the insulin binding to the capturing aptamer was additionally evaluated to exclude unspecific binding to any ssDNA. Therefore, the capability of insulin to associate with the albumin aptamer was investigated. We chose this aptamer since human serum albumin (HSA) is also a diabetes biomarker used for glycemic control. Therefore, multi-analyte aptasensors for diabetes monitoring may be developed in the future that contain aptamers for both analytes (HSA and insulin). Correspondingly, an albumin aptamer/PEG receptor-based aptasensor was fabricated to measure the DPV signals in 5 mM $[Fe(CN)_6]^{3-/4-}$ before and after the incubation of 1 μM insulin as described in our previous work [91]. The response of this sensor was compared with the MB peak alteration of the insulin aptasensor by insulin during SWV measurements in 10 mM PBS. The signal drop of MB for the insulin aptasensor due to the PC-ssDNA replacement was around 80 % while the albumin aptamer/PEG receptor possesses a much smaller signal drop (less than 6 %) (Fig. 4C). This finding indicates a negligible interaction between insulin and the non-analyte-specific ssDNAs which suggests that the development of multi-analyte diabetes sensors containing both aptamers would be feasible.

The stability of the insulin aptasensor was further tested by measuring the I_{AQ}/I_{MB} signal ratios after exposure to 100 nM insulin with a storage time of 1, 2, and 4 weeks in a fridge (Fig. 4D). The recorded signal ratio remained at 83 % even after one month in comparison with that instant measurement just after the modification of the aptasensor (0 weeks). The loss of signal ratio may be attributed to the phase separation and aggregation for aptamers and PEG molecules along with the storage time, which is similar to what was observed for malaria, serotonin, and albumin aptasensors [52,91,92]. Noteworthy, the signal ratio remained more than 90 % after the storage of 2 weeks, which is higher than that of around 80 % after 10 days of storage for albumin aptasensors [91]. This observation can be ascribed to the replacement of the single thiol group by two dithiol-phosphoramidite $(DTPA)_2$ groups for the immobilization of the capturing aptamer, which means that four Au-S bonds facilitated aptamer attachment instead of one. Furthermore, the stronger interaction between the aptamer and the gold surface simultaneously inhibited the phase separation and aggregation between the aptamer and PEG molecules [93–96]. Nevertheless, the prevention of sensor degradation during longtime storage needs to be further addressed in future studies.

4. Conclusion

In summary, in this work, an insulin aptasensor is reported that utilizes a capturing ssDNA aptamer and a partially complementary ssDNA probe both labeled with specific redox tags for an enhanced sensor performance. Therefore, at first, the general fabrication

procedures of the proposed aptasensor were examined by electrochemical impedance spectroscopy, cyclic voltammogram, QCM-D, chronocoulometry, and atomic force microscopy. Afterward, the experimental conditions such as the sequence of the complementary ssDNAs, aptamer concentrations, and target incubation time were optimized. The obtained information was used to establish an insulin aptasensor platform that exhibited high reliability due to the utilization of two redox probes and the implementation of an AND logic gate. The redox probes associated with either the capturing aptamer or the partially complementary-ssDNA facilitated also a wide detection range with two sensitivity regions corresponding to low and relatively high insulin concentrations. In addition, the aptasensor exhibited a high selectivity and recovery performance in diluted blood sample detection, again profiting from the combination of the two redox signals. Another novelty reported in this work was the first-time utilization of linker-free double dithiol-phosphoramidite groups anchored on the capturing aptamer. Polyethylene glycol blocking molecules prevented the unspecific adsorption from the matrix blood samples, thus facilitating the selective determination of the target analyte. Diabetes mellitus is a disease of increasing prevalence and requires lifetime glycemic management, which involves insulin therapy. The capability of monitoring the insulin level affordably and conveniently would significantly improve the treatment for an increasing number of patients in developed and developing nations. The utilization of low-cost and versatile aptamer receptors together with the engineering of ratiometric electrochemical signal recording has the potential to considerably advance the current insulin detection technology toward multi-analyte diabetes sensors. In our previous publication, we have reported on a polymer based multielectrode array (flexMEA), where each electrode can be individually modified and electrically addressed so that every electrode can function as a separate sensor. Here, we envision that the optimized insulin aptasensor can be combined via a multielectrode array platform with other sensors for the detection of diabetes biomarkers such as glucose, HSA/GHSA or HbA1c to achieve a multi-analyte diabetes sensor for improved glycemia control [91,97].

CRediT authorship contribution statement

Lei Zhou: Writing – review & editing, Writing – original draft, Visualization, Validation, Software, Methodology, Investigation, Funding acquisition, Formal analysis, Data curation, Conceptualization. **Ruifeng Zhu:** Writing – review & editing, Validation, Software, Formal analysis, Data curation. **Gabriela Figueroa-Miranda:** Writing – review & editing, Software, Methodology, Formal analysis, Data curation, Conceptualization. **Marc Neis:** Writing – review & editing, Validation, Software, Formal analysis. **Andreas Offenhäusser:** Writing – review & editing, Methodology, Data curation. **Dirk Mayer:** Writing – review & editing, Writing – original draft, Visualization, Validation, Supervision, Software, Resources, Project administration, Methodology, Investigation, Funding acquisition, Formal analysis, Data curation, Conceptualization.

Declaration of competing interest

The authors declare that they have no known competing financial interests or personal relationships that could have appeared to influence the work reported in this paper.

Data availability

Data will be made available on request.

Acknowledgment

L. Zhou gratefully acknowledges financial support from the China Scholarship Council (No. 201708320255).

Appendix A. Supplementary data

Supplementary data to this article can be found online at https://doi.org/10.1016/j.aca.2024.342823.

References

[1] B.A. Perkins, J.L. Sherr, C. Mathieu, Type 1 diabetes glycemic management: insulin therapy, glucose monitoring, and automation, Science (2021) 373, https://doi.org/10.1126/science.abg4502, 1979.
[2] E.K. Spanakis, A. Urrutia, R.J. Galindo, P. Vellanki, A.L. Migdal, G. Davis, M. Fayfman, T. Idrees, F.J. Pasquel, W.Z. Coronado, B. Albury, E. Moreno, L. G. Singh, I. Marcano, S. Lizama, C. Gothong, K. Munir, C. Chesney, R. Maguire, W. H. Scott, M.C. Perez-Guzman, S. Cardona, L. Peng, G.E. Umpierrez, Continuous glucose monitoring–guided insulin administration in hospitalized patients with diabetes: a randomized clinical trial, Diabetes Care 45 (2022), https://doi.org/10.2337/dc22-0716.
[3] F. Sanger, H. Tuppy, The amino-acid sequence in the phenylalanyl chain of insulin. I. The identification of lower peptides from partial hydrolysates, Biochem. J. 49 (1951), https://doi.org/10.1042/bj0490463.
[4] P. Maechler, C.B. Wollhelm, Mitochondrial glutamate acts as a messenger in glucose-induced insulin exocytosis, Nature 402 (1999), https://doi.org/10.1038/45280.
[5] A.J. Scheen, Investigational insulin secretagogues for type 2 diabetes, Expet Opin. Invest. Drugs 25 (2016), https://doi.org/10.1517/13543784.2016.1152260.
[6] S. Del Prato, P. Marchetti, R.C. Bonadonna, Phasic insulin release and metabolic regulation in type 2 diabetes, Diabetes (2002), https://doi.org/10.2337/diabetes.51.2007.s109.
[7] J.R. Speakman, K.D. Hall, Carbohydrates, insulin, and obesity, Science (1979) (2021) 372, https://doi.org/10.1126/science.aav0448.
[8] Ansarullah C. Jain, F.F. Far, S. Homberg, K. Wißmiller, F.G. von Hahn, A. Raducanu, S. Schirge, M. Sterr, S. Bilekova, J. Siehler, J. Wiener, L. Oppenländer, A. Morshedi, A. Bastidas-Ponce, G. Collden, M. Irmler, J. Beckers, A. Feuchtinger, M. Grzybek, C. Ahlbrecht, R. Feederle, O. Plettenburg, T.D. Müller, M. Meier, M.H. Tschöp, Ü. Coskun, H. Lickert, Inceptor counteracts insulin signalling in β-cells to control glycaemia, Nature 590 (2021) 326–331, https://doi.org/10.1038/s41586-021-03225-8.
[9] S. Hædersdal, A. Andersen, F.K. Knop, T. Vilsbøll, Revisiting the role of glucagon in health, diabetes mellitus and other metabolic diseases, Nat. Rev. Endocrinol. (2023), https://doi.org/10.1038/s41574-023-00817-4.
[10] J.R. Zierath, Y. Kawano, The effect of hyperglycaemia on glucose disposal and insulin signal transduction in skeletal muscle, Best Pract. Res. Clin. Endocrinol. Metabol. 17 (2003), https://doi.org/10.1016/S1521-690X(03)00040-X.
[11] A. Virkamäki, K. Ueki, C.R. Kahn, Protein-protein interaction in insulin signaling and the molecular mechanisms of insulin resistance, J. Clin. Invest. 103 (1999), https://doi.org/10.1172/JCI6609.
[12] S. Craft, G.S. Watson, Insulin and neurodegenerative disease: shared and specific mechanisms, Lancet Neurol. 3 (2004), https://doi.org/10.1016/S1474-4422(04)00681-7.
[13] R.J. Perry, G.I. Shulman, Mechanistic links between obesity, insulin, and cancer, Trends Cancer 6 (2020), https://doi.org/10.1016/j.trecan.2019.12.003.
[14] S. Lablanche, M.C. Vantyghem, L. Kessler, A. Wojtusciszyn, S. Borot, C. Thivolet, S. Girerd, D. Bosco, J.L. Bosson, C. Colin, R. Tetaz, S. Logerot, J. Kerr-Conte, E. Renard, A. Penfornis, E. Morelon, F. Buron, K. Skaare, G. Grguric, C. Camillo-Brault, H. Egelhofer, K. Benomar, L. Badet, T. Berney, F. Pattou, P.Y. Benhamou, P. Malvezzi, I. Tauveron, B. Roche, C. Noel, L. Frimat, B. Guerci, N. Pernin, A. Moisan, V. Persoons, R. Ezzouaoui, V. Gmyr, F. Thony, Y. Bricault, M. Rodière, C. Sengel, M. Greget, I. Enescu, M. Hazzan, R. Caiazzo, F. Torres, K. Le Mapihan, V. Raverdy, M.A. Pierredon, P.J. Valette, A. Muller, J. Champagnac, L. Chaillous, J. Dantal, P. Cattan, J.P. Riveline, F. Moreau, P. Baltzinger, T. Bahoune, Islet transplantation versus insulin therapy in patients with type 1 diabetes with severe hypoglycaemia or poorly controlled glycaemia after kidney transplantation (TRIMECO): a multicentre, randomised controlled trial, Lancet Diabetes Endocrinol. 6 (2018), https://doi.org/10.1016/S2213-8587(18)30078-0.
[15] A. Breenfeldt Andersen, G.A. Jacobson, J. Bejder, D. Premilovac, S.M. Richards, J. J. Rasmussen, S. Jessen, M. Hostrup, An abductive inference approach to assess the performance-enhancing effects of drugs included on the world anti-doping agency prohibited list, Sports Med. 51 (2021) 1353–1376, https://doi.org/10.1007/s40279-021-01450-9.
[16] A.D. Rogol, L.M. Laffel, B. Bode, M.A. Sperling, Celebration of a century of insulin therapy in children with type 1 diabetes, Arch. Dis. Child. 108 (2022), https://doi.org/10.1136/archdischild-2022-323975.
[17] P.V. Ferdowsi, K.D.K. Ahuja, J.M. Beckett, S. Myers, Capsaicin and zinc signalling pathways as promising targets for managing insulin resistance and type 2 diabetes, Molecules 28 (2023) 1–16, https://doi.org/10.3390/molecules28062861.
[18] H. Cho, S. Kumar, D. Yang, S. Vaidyanathan, K. Woo, I. Garcia, H.J. Shue, Y. Yoon, K. Ferreri, H. Choo, Surface-enhanced Raman spectroscopy-based label-free insulin detection at physiological concentrations for analysis of islet performance, ACS Sens. 3 (2018), https://doi.org/10.1021/acssensors.7b00864.
[19] V. Singh, S. Krishnan, Electrochemical and surface plasmon insulin assays on clinical samples, Analyst 143 (2018), https://doi.org/10.1039/c7an01872j.
[20] I. Šišoláková, J. Hovancová, F. Chovancová, R. Oriňaková, I. Maskaľová, A. Oriňak, J. Radoňak, Zn nanoparticles modified screen printed carbon electrode as a

promising sensor for insulin determination, Electroanalysis 33 (2021) 627–634, https://doi.org/10.1002/elan.202060417.
[21] D.F. Kruger, M.A. Gloster, Pramlintide for the treatment of insulin-requiring diabetes mellitus: rationale and review of clinical data, Drugs 64 (2004), https://doi.org/10.2165/00003495-200464130-00003.
[22] D. Kerr, S. Edelman, G. Vespasiani, K. Khunti, New digital health technologies for insulin initiation and optimization for people with type 2 diabetes, Endocr. Pract. 28 (2022), https://doi.org/10.1016/j.eprac.2022.04.006.
[23] I. Cranston, J. Lomas, S.A. Amiel, A. Maran, I. Macdonald, Restoration of hypoglycaemia awareness in patients with long-duration insulin-dependent diabetes, Lancet 344 (1994), https://doi.org/10.1016/S0140-6736(94)91336-6.
[24] M.E. Røder, B. Dinesen, F. Poulsen, Measurement of Insulin Immunoreactivity in Human Plasma and Serum, vol. 1426, 2009, pp. 1425–1426, https://doi.org/10.1373/clinchem.2009.126102.
[25] J. Wang, A. Ibáñez, M.P. Chatrathi, A. Escarpa, Electrochemical enzyme immunoassays on microchip platforms, Anal. Chem. 73 (2001) 5323–5327, https://doi.org/10.1021/ac010808h.
[26] H. Ma, X. Li, T. Yan, Y. Li, H. Liu, Y. Zhang, D. Wu, B. Du, Q. Wei, Sensitive insulin detection based on electrogenerated chemiluminescence resonance energy transfer between Ru(bpy)32+ and Au nanoparticle-doped β-cyclodextrin-Pb (II) metal-organic framework, ACS Appl. Mater. Interfaces 8 (2016) 10121–10127, https://doi.org/10.1021/acsami.5b11991.
[27] C. Chanussot, L. Bellanger, C. Ligny-Lemaire, P. Seguin, A. Ménez, J.C. Boulain, Engineering of a recombinant colorimetric fusion protein for immunodiagnosis of insulin, J. Immunol. Methods 197 (1996) 39–49, https://doi.org/10.1016/0022-1759(96)00109-3.
[28] P.L. Andersen, P. Vermette, Intracellular insulin quantification by cell-ELISA, Exp. Cell Res. 347 (2016), https://doi.org/10.1016/j.yexcr.2016.06.014.
[29] M. Poudineh, C.L. Maikawa, E.Y. Ma, J. Pan, D. Mamerow, Y. Hang, S.W. Baker, A. Beirami, A. Yoshikawa, M. Eisenstein, S. Kim, J. Vučković, E.A. Appel, H.T. Soh, A fluorescence sandwich immunoassay for the real-time continuous detection of glucose and insulin in live animals, Nat. Biomed. Eng. 5 (2021), https://doi.org/10.1038/s41551-020-00661-1.
[30] M. Frasconi, C. Tortolini, F. Botrè, F. Mazzei, Multifunctional Au nanoparticle dendrimer-based surface plasmon resonance biosensor and its application for improved insulin detection, Anal. Chem. 82 (2010), https://doi.org/10.1021/ac101319k.
[31] Y. Sakaguchi, T. Kinumi, A. Takatsu, A dual functional-group derivatization liquid chromatography–tandem mass spectrometry method: application for quantification of human insulin, Chromatographia 85 (2022), https://doi.org/10.1007/s10337-022-04136-0.
[32] M.M. Moein, M. Javanbakht, B. Akbari-Adergani, Molecularly imprinted polymer cartridges coupled on-line with high performance liquid chromatography for simple and rapid analysis of human insulin in plasma and pharmaceutical formulations, Talanta 121 (2014), https://doi.org/10.1016/j.talanta.2013.12.011.
[33] N. Hamidli, B. Pajaziti, M. Andrási, C. Nagy, A. Gáspár, Determination of human insulin and its six therapeutic analogues by capillary electrophoresis – mass spectrometry, J. Chromatogr. A 1678 (2022), https://doi.org/10.1016/j.chroma.2022.463351.
[34] H. Teymourian, A. Barfidokht, J. Wang, Electrochemical glucose sensors in diabetes management: an updated review (2010-2020), Chem. Soc. Rev. 49 (2020) 7671–7709, https://doi.org/10.1039/d0cs00304b.
[35] Y.M. Park, Y.S. Choi, H.R. Lee, Y.S. Heo, N.H. Bae, T.J. Lee, S.J. Lee, Flexible and highly ordered nanopillar electrochemical sensor for sensitive insulin evaluation, Biosens. Bioelectron. 161 (2020), https://doi.org/10.1016/j.bios.2020.112252.
[36] M. Khanwalker, R. Fujita, J. Lee, E. Wilson, K. Ito, R. Asano, K. Ikebukuro, J. LaBelle, K. Sode, Development of a POCT type insulin sensor employing anti-insulin single chain variable fragment based on faradaic electrochemical impedance spectroscopy under single frequency measurement, Biosens. Bioelectron. 200 (2022), https://doi.org/10.1016/j.bios.2021.113901.
[37] H. Ausserwöger, M.M. Schneider, T.W. Herling, P. Arosio, G. Invernizzi, T.P. J. Knowles, N. Lorenzen, Non-specificity as the sticky problem in therapeutic antibody development, Nat. Rev. Chem 6 (2022), https://doi.org/10.1038/s41570-022-00438-x.
[38] M. Xiao, W. Lai, T. Man, B. Chang, L. Li, A.R. Chandrasekaran, H. Pei, Rationally engineered nucleic acid architectures for biosensing applications, Chem. Rev. 119 (2019), https://doi.org/10.1021/acs.chemrev.9b00121.
[39] S. Qi, N. Duan, I.M. Khan, X. Dong, Y. Zhang, S. Wu, Z. Wang, Strategies to manipulate the performance of aptamers in SELEX, post-SELEX and microenvironment, Biotechnol. Adv. 55 (2022), https://doi.org/10.1016/j.biotechadv.2021.107902.
[40] W. Yoshida, E. Mochizuki, M. Takase, H. Hasegawa, Y. Morita, H. Yamazaki, K. Sode, K. Ikebukuro, Selection of DNA aptamers against insulin and construction of an aptameric enzyme subunit for insulin sensing, Biosens. Bioelectron. 24 (2009), https://doi.org/10.1016/j.bios.2008.06.016.
[41] Z. Hao, Y. Zhu, X. Wang, P.G. Rotti, C. Dimarco, S.R. Tyler, X. Zhao, J. F. Engelhardt, J. Hone, Q. Lin, Real-time monitoring of insulin using a graphene field-effect transistor aptameric nanosensor, ACS Appl. Mater. Interfaces 9 (2017) 27504–27511, https://doi.org/10.1021/acsami.7b07684.
[42] M. Liu, H. Zhao, S. Chen, H. Yu, X. Quan, Interface engineering catalytic graphene for smart colorimetric biosensing, ACS Nano 6 (2012) 3142–3151, https://doi.org/10.1021/nn3010922.
[43] Y. Wu, B. Midinov, R.J. White, Electrochemical aptamer-based sensor for real-Time monitoring of insulin, ACS Sens. 4 (2019), https://doi.org/10.1021/acssensors.8b01573.
[44] M. Amouzadeh Tabrizi, M. Shamsipur, R. Saber, S. Sarkar, M. Besharati, An electrochemical aptamer-based assay for femtomolar determination of insulin using a screen printed electrode modified with mesoporous carbon and 1,3,6,8-pyrenetetrasulfonate, Microchim. Acta 185 (2018), https://doi.org/10.1007/s00604-017-2570-z.
[45] R. Sakthivel, L.Y. Lin, Y.F. Duann, H.H. Chen, C. Su, X. Liu, J.H. He, R.J. Chung, MOF-derived Cu-btc nanowire-embedded 2D leaf-like structured ZIF composite-based aptamer sensors for real-time in vivo insulin monitoring, ACS Appl. Mater. Interfaces 14 (2022) 28639–28650, https://doi.org/10.1021/acsami.2c06785.
[46] J. Liu, B. Zhu, H. Dong, Y. Zhang, M. Xu, J. Travas-Sejdic, Z. Chang, A novel electrochemical insulin aptasensor: from glassy carbon electrodes to disposable, single-use laser-scribed graphene electrodes, Bioelectrochemistry 143 (2022) 107995, https://doi.org/10.1016/j.bioelechem.2021.107995.
[47] Y. Zhao, Y. Xu, M. Zhang, J. Xiang, C. Deng, H. Wu, An electrochemical dual-signaling aptasensor for the ultrasensitive detection of insulin, Anal. Biochem. 573 (2019), https://doi.org/10.1016/j.ab.2019.02.032.
[48] Z. Chen, C. Liu, X. Su, W. Zhang, X. Zou, Signal on-off ratiometric electrochemical sensor based on semi-complementary aptamer couple for sensitive cadmium detection in mussel, Sensor. Actuator. B Chem. 346 (2021), https://doi.org/10.1016/j.snb.2021.130506.
[49] N. Meini, C. Farre, C. Chaix, R. Kherrat, S. Dzyadevych, N. Jaffrezic-Renault, A sensitive and selective thrombin impedimetric aptasensor based on tailored aptamers obtained by solid-phase synthesis, Sensor. Actuator. B Chem. (2012) 166–167, https://doi.org/10.1016/j.snb.2012.03.046.
[50] M. Takenaka, Y. Okumura, T. Amino, Y. Miyachi, C. Ogino, A. Kondo, DNA-duplex linker for AFM-SELEX of DNA aptamer against human serum albumin, Bioorg. Med. Chem. Lett 27 (2017) 954–957, https://doi.org/10.1016/j.bmcl.2016.12.080.
[51] F. Schröper, D. Brüggemann, Y. Mourzina, B. Wolfrum, A. Offenhäusser, D. Mayer, Analyzing the electroactive surface of gold nanopillars by electrochemical methods for electrode miniaturization, Electrochim. Acta 53 (2008), https://doi.org/10.1016/j.electacta.2008.03.068.
[52] G. Figueroa-Miranda, C. Wu, Y. Zhang, L. Nörbel, Y. Lo, J.A. Tanner, L. Elling, A. Offenhäusser, D. Mayer, Polyethylene glycol-mediated blocking and monolayer morphology of an electrochemical aptasensor for malaria biomarker detection in human serum, Bioelectrochemistry 136 (2020), https://doi.org/10.1016/j.bioelechem.2020.107589.
[53] S. Schmidt, K. Uhlig, C. Duschl, D. Volodkin, Stability and cell uptake of calcium carbonate templated insulin microparticles, Acta Biomater. 10 (2014), https://doi.org/10.1016/j.actbio.2013.11.011.
[54] O. Wintersteiner, H.A. Abramson, The isoelectric point of insulin, J. Biol. Chem. 99 (1933), https://doi.org/10.1016/s0021-9258(18)76023-7.
[55] L. Langkjær, J. Brange, G.M. Grodsky, R.H. Guy, Iontophoresis of monomeric insulin analogues in vitro: effects of insulin charge and skin pretreatment, J. Contr. Release 51 (1998), https://doi.org/10.1016/S0168-3659(97)00155-7.
[56] Z. Adamczyk, M. Sadowska, P. Żeliszewska, Applicability of QCM-D for quantitative measurements of nano- and microparticle deposition kinetics: theoretical modeling and experiments, Anal. Chem. 92 (2020), https://doi.org/10.1021/acs.analchem.0c03115.
[57] G. Sauerbrey, Verwendung von Schwingquarzen zur Wägung dünner Schichten und zur Mikrowägung, Z. Phys. 155 (1959), https://doi.org/10.1007/BF01337937.
[58] A.B. Steel, R.L. Levicky, T.M. Herne, M.J. Tarlov, Immobilization of nucleic acids at solid surfaces : effect of oligonucleotide length on layer assembly, Biophys. J. 79 (2000) 975–981, https://doi.org/10.1016/S0006-3495(00)76351-X.
[59] A.B. Steel, T.M. Herne, M.J. Tarlov, Electrochemical quantitation of DNA immobilized on gold, Anal. Chem. 70 (1998), https://doi.org/10.1021/ac980037q.
[60] D. Zhou, K. Sinniah, C. Abell, T. Rayment, Use of atomic force microscopy for making addresses in DNA coatings, Langmuir 18 (2002) 8278–8281, https://doi.org/10.1021/la0258547.
[61] T.M. Herne, M.J. Tarlov, Characterization of DNA probes immobilized on gold surfaces, J. Am. Chem. Soc. 119 (1997), https://doi.org/10.1021/ja9719586.
[62] C. Wu, D. Barkova, N. Komarova, A. Offenhäusser, M. Andrianova, Z. Hu, A. Kuznetsov, D. Mayer, Highly selective and sensitive detection of glutamate by an electrochemical aptasensor, Anal. Bioanal. Chem. 414 (2022), https://doi.org/10.1007/s00216-021-03783-w.
[63] Y. Zhang, G. Figueroa-Miranda, C. Zafiu, D. Willbold, A. Offenhäusser, D. Mayer, Amperometric aptasensor for amyloid-β oligomer detection by optimized stem-loop structures with an adjustable detection range, ACS Sens. 4 (2019) 3042–3050, https://doi.org/10.1021/acssensors.9b01630.
[64] J. Zhang, S. Song, L. Wang, D. Pan, C. Fan, A gold nanoparticle-based chronocoulometric dna sensor for amplified detection of dna, Nat. Protoc. 2 (2007) 2888–2895, https://doi.org/10.1038/nprot.2007.419.
[65] Z. Zhang, C. Tao, Rational design of a mismatched aptamer-DNA duplex probe to improve the analytical performance of electrochemical aptamer sensors, Electrochim. Acta 209 (2016), https://doi.org/10.1016/j.electacta.2016.05.107.
[66] B. Soontornworajit, J. Zhou, M.P. Snipes, M.R. Battig, Y. Wang, Affinity hydrogels for controlled protein release using nucleic acid aptamers and complementary oligonucleotides, Biomaterials 32 (2011), https://doi.org/10.1016/j.biomaterials.2011.05.074.
[67] J. Zhou, B. Soontornworajit, M.P. Snipes, Y. Wang, Structural prediction and binding analysis of hybridized aptamers, J. Mol. Recogn. 24 (2011), https://doi.org/10.1002/jmr.1034.
[68] L. Le Wang, Y. Wen, L. Li, X. Yang, N. Jia, W. Li, J. Meng, M. Duan, X. Sun, G. Liu, Sensitive and label-free electrochemical lead ion biosensor based on a DNAzyme

triggered G-quadruplex/hemin conformation, Biosens. Bioelectron. 115 (2018), https://doi.org/10.1016/j.bios.2018.04.054.
[69] G. Wang, L. Chen, Y. Zhu, X. He, G. Xu, X. Zhang, Development of an electrochemical sensor based on the catalysis of ferrocene actuated hemin/G-quadruplex enzyme for the detection of potassium ions, Biosens. Bioelectron. 61 (2014), https://doi.org/10.1016/j.bios.2014.05.052.
[70] B. Lenyk, G. Figueroa-Miranda, I. Pavlushko, Y. Lo, J.A. Tanner, A. Offenhäusser, D. Mayer, Dual-transducer malaria aptasensor combining electrochemical impedance and surface plasmon polariton detection on gold nanohole arrays, Chemelectrochem 7 (2020) 4594–4600, https://doi.org/10.1002/celc.202001212.
[71] G. Figueroa-Miranda, L. Feng, S.C.C. Shiu, R.M. Dirkzwager, Y.W. Cheung, J. A. Tanner, M.J. Schöning, A. Offenhäusser, D. Mayer, Aptamer-based electrochemical biosensor for highly sensitive and selective malaria detection with adjustable dynamic response range and reusability, Sensor. Actuator. B Chem. 255 (2018) 235–243, https://doi.org/10.1016/j.snb.2017.07.117.
[72] M.F. Saad, D.J. Pettitt, D.M. Mott, W.C. Knowler, R.G. Nelson, P.H. Bennett, Sequential changes in serum insulin concentration during development OF NON-INSULIN-DEPENDENT diabetes, Lancet 333 (1989), https://doi.org/10.1016/S0140-6736(89)92804-3.
[73] C. Gu, Y. Liu, B. Hu, Y. Liu, N. Zhou, L. Xia, Z. Zhang, Multicomponent nanohybrids of nickel/ferric oxides and nickel cobaltate spinel derived from the MOF-on-MOF nanostructure as efficient scaffolds for sensitively determining insulin, Anal. Chim. Acta 1110 (2020) 44–55, https://doi.org/10.1016/j.aca.2020.03.019.
[74] J. Chen, Z. Liu, R. Yang, M. Liu, H. Feng, N. Li, M. Jin, M. Zhang, L. Shui, A liquid crystal-based biosensor for detection of insulin driven by conformational change of an aptamer at aqueous-liquid crystal interface, J. Colloid Interface Sci. 628 (2022), https://doi.org/10.1016/j.jcis.2022.07.051.
[75] F. Abazar, E. Sharifi, A. Noorbakhsh, Antifouling properties of carbon quantum dots-based electrochemical sensor as a promising platform for highly sensitive detection of insulin, Microchem. J. 180 (2022), https://doi.org/10.1016/j.microc.2022.107560.
[76] J. Shepa, I. Šišoláková, M. Vojtko, L. Trnková, G. Nagy, I. Maskaľová, A. Oriňak, R. Oriňaková, Nio nanoparticles for electrochemical insulin detection, Sensors 21 (2021), https://doi.org/10.3390/s21155063.
[77] F. Asadpour, M. Mazloum-Ardakani, F. Hoseynidokht, S.M. Moshtaghioun, In situ monitoring of gating approach on mesoporous silica nanoparticles thin-film generated by the EASA method for electrochemical detection of insulin, Biosens. Bioelectron. 180 (2021), https://doi.org/10.1016/j.bios.2021.113124.
[78] H. Razmi, L. Ezzati, Z. Khorablou, Direct electrochemical synthesis of graphene oxide/cobalt oxide nanocomposite on pencil graphite electrode for highly sensitive and selective detection of insulin in pharmaceutical samples, J. Electrochem. Soc. 166 (2019), https://doi.org/10.1149/2.0621912jes.
[79] S. Tan, R. Han, S. Wu, H. Liang, Y. Zhao, H. Zhao, C.P. Li, A novel fluorescent sensing platform for insulin detection based on competitive recognition of cationic pillar[6]arene, Talanta 197 (2019), https://doi.org/10.1016/j.talanta.2019.01.004.
[80] R. Chhasatia, M.J. Sweetman, B. Prieto-Simon, N.H. Voelcker, Performance optimisation of porous silicon rugate filter biosensor for the detection of insulin, Sensor. Actuator. B Chem. 273 (2018), https://doi.org/10.1016/j.snb.2018.07.021.
[81] J. Yang, Z. Zhang, G. Yan, An aptamer-mediated CdSe/ZnS QDs@graphene oxid composite fluorescent probe for specific detection of insulin, Sensor. Actuator. B Chem. 255 (2018), https://doi.org/10.1016/j.snb.2017.09.046.
[82] R. Chhasatia, M.J. Sweetman, F.J. Harding, M. Waibel, T. Kay, H. Thomas, T. Loudovaris, N.H. Voelcker, Non-invasive, in vitro analysis of islet insulin production enabled by an optical porous silicon biosensor, Biosens. Bioelectron. 91 (2017), https://doi.org/10.1016/j.bios.2017.01.004.
[83] Z.J. Farino, T.J. Morgenstern, J. Vallaghe, N. Gregor, P. Donthamsetti, P.E. Harris, N. Pierre, R. Freyberg, F. Charrier-Savournin, J.A. Javitch, Z. Freyberg, Development of a rapid insulin assay by homogenous time-resolved fluorescence, PLoS One 11 (2016), https://doi.org/10.1371/journal.pone.0148684.
[84] M.S. Even, C.B. Sandusky, N.D. Barnard, J. Mistry, M.K. Sinha, Development of a novel ELISA for human insulin using monoclonal antibodies produced in serum-free cell culture medium, Clin. Biochem. 40 (2007), https://doi.org/10.1016/j.clinbiochem.2006.10.004.
[85] R. Abellan, R. Ventura, I. Palmi, S. di Carlo, R. di Giovannandrea, M. Bellver, R. Olive, J.A. Pascual, R. Pacifici, J. Segura, P. Zuccaro, S. Pichini, Evaluation of immunoassays for the measurement of insulin and C-peptide as indirect biomarkers of insulin misuse in sport: values in selected population of athletes, J. Pharm. Biomed. Anal. 49 (2009), https://doi.org/10.1016/j.jpba.2008.12.037.
[86] K. Brummel-Ziedins, C.Y. Vossen, F.R. Rosendaal, K. Umezaki, K.G. Mann, The plasma hemostatic proteome: thrombin generation in healthy individuals, J. Thromb. Haemostasis 3 (2005), https://doi.org/10.1111/j.1538-7836.2005.01249.x.
[87] M.J.A.J. Huijskens, W.K.W.H. Wodzig, M. Walczak, W.T.V. Germeraad, G.M.J. Bos, Ascorbic acid serum levels are reduced in patients with hematological malignancies, Results Immunol. 6 (2016), https://doi.org/10.1016/j.rinim.2016.01.001.
[88] S.A. Alex, S. Rajiv, S. Chakravarty, N. Chandrasekaran, A. Mukherjee, Significance of surface functionalization of Gold Nanorods for reduced effect on IgG stability and minimization of cytotoxicity, Mater. Sci. Eng. C 71 (2017) 744–754, https://doi.org/10.1016/j.msec.2016.10.061.
[89] A. Gonzalez-Quintela, R. Alende, F. Gude, J. Campos, J. Rey, L.M. Meijide, C. Fernandez-Merino, C. Vidal, Serum levels of immunoglobulins (IgG, IgA, IgM) in a general adult population and their relationship with alcohol consumption, smoking and common metabolic abnormalities, Clin. Exp. Immunol. 151 (2008), https://doi.org/10.1111/j.1365-2249.2007.03545.x.
[90] M.P. Brigham, W.H. Stein, S. Moore, The concentrations of cysteine and cystine in human blood plasma, J. Clin. Invest. 39 (1960), https://doi.org/10.1172/jci104186.
[91] L. Zhou, G. Figueroa-Miranda, S. Chen, M. Neis, Z. Hu, R. Zhu, Y. Li, M. Prömpers, A. Offenhäusser, D. Mayer, Flexible multielectrode arrays based electrochemical aptasensor for glycated human serum albumin detection, Sensor. Actuator. B Chem. 386 (2023), https://doi.org/10.1016/j.snb.2023.133730.
[92] Z. Hu, R. Zhu, G. Figueroa-Miranda, L. Zhou, L. Feng, A. Offenhäusser, D. Mayer, Truncated electrochemical aptasensor with enhanced antifouling capability for highly sensitive serotonin detection, Biosensors 13 (2023) 881, https://doi.org/10.3390/bios13090881.
[93] P. Liepold, T. Kratzmüller, N. Persike, M. Bandilla, M. Hinz, H. Wieder, H. Hillebrandt, E. Ferrer, G. Hartwich, Electrically detected displacement assay (EDDA): a practical approach to nucleic acid testing in clinical or medical diagnosis, Anal. Bioanal. Chem. 391 (2008), https://doi.org/10.1007/s00216-008-2045-5.
[94] D.H. Paik, Yeonee Seol, W.A. Halsey, T.T. Perkins, Integrating a high-force optical trap with gold nanoposts and a robust gold-dna bond, Nano Lett. 9 (2009) 2978–2983, https://doi.org/10.1021/nl901404s.
[95] M. Sajfutdinow, K. Uhlig, A. Prager, C. Schneider, B. Abel, D.M. Smith, Nanoscale patterning of self-assembled monolayer (SAM)-functionalised substrates with single molecule contact printing, Nanoscale 9 (2017), https://doi.org/10.1039/c7nr03696e.
[96] N. Meini, M. Ripert, C. Chaix, C. Farre, G. De Crozals, R. Kherrat, N. Jaffrezic-Renault, Label-free electrochemical monitoring of protein addressing through electroactivated “click” chemistry on gold electrodes, Mater. Sci. Eng. C 38 (2014), https://doi.org/10.1016/j.msec.2014.02.013.
[97] C. Voulgari, N. Tentolouris, The performance of a glucose-ketone meter in the diagnosis of diabetic ketoacidosis in patients with type 2 diabetes in the emergency room, Diabetes Technol. Therapeut. 12 (2010), https://doi.org/10.1089/dia.2010.0011.